

Durham Research Online

Deposited in DRO:

02 June 2008

Version of attached file:

Accepted Version

Peer-review status of attached file:

Peer-reviewed

Citation for published item:

Petkovski, M. and Crouch, R. S. and Waldron, P. (2006) 'Apparatus for testing concrete under multiaxial compression at elevated temperature (mac2T).', *Experimental mechanics.*, 46 (3). pp. 387-398.

Further information on publisher's website:

<http://dx.doi.org/10.1007/s11340-006-7463-8>

Publisher's copyright statement:

The original publication is available at <http://www.springerlink.com/>

Use policy

The full-text may be used and/or reproduced, and given to third parties in any format or medium, without prior permission or charge, for personal research or study, educational, or not-for-profit purposes provided that:

- a full bibliographic reference is made to the original source
- a [link](#) is made to the metadata record in DRO
- the full-text is not changed in any way

The full-text must not be sold in any format or medium without the formal permission of the copyright holders.

Please consult the [full DRO policy](#) for further details.

4 Apparatus for Testing Concrete under Multiaxial Compression 5 at Elevated Temperature (mac^{2T})

6 M. Petkovski · R.S. Crouch · P. Waldron

7 Received: 23 August 2005 / Accepted: 27 January 2006 / Published online: ■
8 © Society for Experimental Mechanics 2006

11 **Abstract** This paper describes a new test facility for
12 determining material mechanical properties of struc-
13 tural concrete. The novel facility subjects 100 mm
14 cubic concrete specimens to true multiaxial compres-
15 sion ($\sigma_1 \neq \sigma_2 \neq \sigma_3$) up to 400 MPa at temperatures of
16 up to 300°C. Forces are delivered through three
17 independent loading frames equipped with servo-
18 controlled hydraulic actuators creating uniform dis-
19 placement boundary conditions via rigid platens.
20 Specimen deformation is calculated from displace-
21 ments measured to an accuracy of 10^{-6} m using a
22 system of six laser interferometers. The combination of
23 stiff loading frames, rigid platens, an accurate and
24 reliable strain measurement system and a fast control
25 system enables investigation of the material response
26 in the post-peak range. The in-house developed con-
27 trol software allows complex multi-stage experiments
28 involving (i) load and temperature cycling, (ii) small
29 stress probes and (iii) arbitrary (pre-defined) loading
30 paths. The program also enables experiments in which
31 the values of the control parameters and the execution
32 of the test sequences depend on the response of the
33 specimen during the test. The capabilities of the
34 facility are illustrated in this paper by experiments
35 determining the effects of different heat-load regimes
36 on the strength and stiffness of the material and tests
37 identifying the tangent stiffness matrix of the material
38 and the associated changes in the acoustic tensor under
39 multiaxial compression.

40 **Keywords** Test facility · Multiaxial compression ·
41 Concrete · Elevated temperature

Introduction

The lack of a comprehensive database of stress and strain measurements on structural concrete under true multiaxial compression is one of the main obstacles preventing the development of reliable constitutive models for this important engineering material. Current design methods typically assume that the concrete in a column, beam or slab-like structural member is under essentially a uniaxial state of stress. The one-dimensional stress-strain relationship under such conditions is often idealised as following a parabolic form, broadly fitting data from uniaxial compression tests. However, in many safety-critical structures (such as nuclear reactor vessels, nuclear containment vessels, offshore platforms and arch-gravity dams) the stress state is most certainly not uniaxial throughout. Engineering precision and understanding is lost when the effects of confinement and the deformation behaviour in the other two principal directions are ignored. Furthermore, a constitutive model embracing the full three-dimensional behaviour is a requirement when attempting accurate continuum FE simulations.

Although the differences between the uniaxial and biaxial compressive strengths are not so marked, the fracture modes can be quite different [1-3]. Yet it is when all three principal stresses are compressive that very significant differences in strength, deformation and apparent ductility are seen. Most of the knowledge on the behaviour of concrete under multiaxial compression has been gathered from axisymmetric triaxial tests on cylindrical specimens. Triaxial rigs using the Hoek cell [4], originally developed for testing rock, provide simple and inexpensive devices that have proved popular for researchers investigating the response of concrete under confinement [5-7]. Newman's triaxial

Q1 M. Petkovski (✉) · R.S. Crouch · P. Waldron
The University of Sheffield
e-mail: m.petkovski@sheffield.ac.uk

compression and extension tests [8], carried out in a specially designed apparatus operating at higher pressures, revealed the dramatic effect of confinement on the stress-strain nonlinearity of concrete. The strains he measured at peak stress were over 57 times larger than those seen under uniaxial compression. The triaxial cell tests performed by Jamet et al. [9] showed that with the increase of confinement the post-peak behaviour of micro-concrete gradually changed from brittle to ductile. Similar change in behaviour was observed in tests on concretes with three different strengths carried out in the Colorado triaxial cell [10]. These tests indicated that for higher strength concretes the transition from brittle to ductile behaviour occurred at higher levels of confinement. In 1999 Lee and Ansari [11] calibrated their constitutive model using data from tests on high-strength concrete in a cell allowing up to 83 MPa confinement and 574 MPa axial stress. In 2002 Sfer et al. [12] tested larger (150 mm diameter, 300 mm long) cylinders in a triaxial cell with a capacity of 4.5 MN axial load and 140 MPa confinement pressure. These tests confirmed the transition from brittle to ductile behaviour and suggested that with the increase of confinement the rupture mode changed from a diffuse distribution of microcracks to a mechanism involving fewer macrocracks separating the specimen into two or three blocks. This was in contrast to the earlier findings of Newman, which suggests that a particular care is needed in interpreting the effects of the boundary conditions at the specimen-platen interface. Other triaxial cells introducing improvements of the original Hoek Cell design include the facilities in Milan and Bergamo [13] and the recently developed GIGA triaxial cell in Grenoble, a rig capable of delivering up to 2500 MPa axial stress on 70 mm diameter, 140 mm long cylindrical specimen, at confinements of up to 850 MPa [14].

While providing important information on the effect of confinement, the triaxial cells are constrained to operate on the compression and extension meridians (that is, the Lode angle is either $+\pi/6$ or $-\pi/6$). The first efforts in true multiaxial compression testing of concrete were made over thirty-five years ago by researchers at the University of New Mexico [15]. They developed an apparatus comprising three independent frames with rigid platens, using polyethylene pads and grease to reduce the platen constraint. Manually operated, pressure controlled actuators with a load capacity of 270 kN were used to test 57 mm cubic specimens under stresses of up to 105 MPa. These findings were valuable, although comparisons with conventional triaxial results suggested that the New Mexico rig did not adequately remove platen friction. In the most comprehensive study of concrete under true

multiaxial compression, Scavuzzo [16] performed tests in a fluid platen rig at the University of Colorado. In addition to simple triaxial compression, triaxial extension and multiaxial compression with three different principal stresses, the cubic specimens were tested under cyclic, staircase, piecewise-uniaxial and circular loading paths. However, the Colorado stress-controlled rig was unable to capture any possible strain softening in the material. The stress range of this impressive apparatus was further limited by the use of leather pads inserted between the fluid cushions and the concrete specimens, which led to stress concentration and development of diagonal cracks near the corners of the specimens at relatively low stress levels. It was at the University of Eindhoven that the post-peak response of conventional structural concrete was captured using brush platens within a rig employing three suspended independent loading frames [17]. Although only a few experiments close to the biaxial regime were reported, that careful work clarified the role of local fragmentation and macroscopic dilation on the loss of load-carrying capacity. The results obtained from using different boundary conditions in the Eindhoven rig suggested that PTFE-coated platens provided the lowest friction restraint in the post-peak region [18].

If there exists limited multiaxial data under ambient conditions, then the position is far worse under elevated temperature. The majority of the experiments performed on hot specimens have been restricted to uniaxial compression. The exceptions are the biaxial studies performed in Braunschweig [19, 20] and the 8 torsional confined cylinder tests at Northwestern University [21]. In the latter tests, the aim was to identify the short-term creep response under controlled moisture conditions at temperatures of up to 200°C. Cylindrical specimens with 152 mm diameter were loaded under axial compression (< 10 MPa), lateral confinement (< 10 MPa) and torsionally induced shear (< 4 MPa). Although these experiments were operating in the relatively low-stress range, the apparatus has the capacity to deliver an axial load of 5 MN, a torque of 5.6 kNm and a fluid cell pressure of 138 MPa.

This lack of data on concrete under high levels of multiaxial compression at elevated temperature led to the development of mac^{2T} , the new experimental rig at The University of Sheffield (Fig. 1).

Test Facility for Multi-Axial Compression of Concrete at Elevated Temperature (mac^{2T})

The apparatus for Multi-Axial Compression of Concrete at Elevated Temperature ($\text{mac} \rightarrow \text{mac}^{2T}$; pro-



Fig. 1. mac^{2T} apparatus for multi-axial compression of concrete at elevated temperature

nounced *masset*) was designed to satisfy four key testing criteria:

- (i) Multi-axial compression of 100 mm cubic specimens up to 400 MPa at any Lode angle ($\sigma_1 \neq \sigma_2 \neq \sigma_3$). Delivery of stresses up to 400 MPa was required to allow structural concretes of the type used in existing nuclear power plant reactor and containment vessels (typical uniaxial compressive strength $f_c = 50\text{--}60$ MPa) to be loaded to peak under high levels of hydrostatic confinement (over 100 MPa). The specimen size was fixed at 100 mm to ensure that a representative volume was tested when using 20 mm coarse aggregate. These constraints led to a design solution incorporating three independent loading frames each of 4 MN load capacity.
- (ii) Ability to test in the post-peak range. Valuable information on the effective ductility and fracture energy can be obtained by monitoring the post-peak response. However, once the maximum stress is attained, there can be a sudden release of energy stored in the loading frames and the specimen. This can lead to an uncontrollable disintegration of the specimen, with loss of load and displacement measurements. In mac^{2T} this effect was minimised by using a combination of compact, stiff loading frames (reducing the elongation of the tensile bars and bending of the

crossheads) and a fast, displacement-controlled servo-hydraulic system that is able to unload the actuators rapidly as the specimen fragments. A disadvantage of rigs where displacements are measured using strain gages bonded to the specimen surface (typical for triaxial cells) is that the large cracks that develop in the post-peak range can fracture the gauges, or local spalling occurs leaving the gauge intact but useless in terms of capturing the global response. This is avoided in mac^{2T} by using un-interruptible laser interferometers that allow an accurate, continuous displacement signal throughout the test.

- (iii) Multi-axial compression at temperatures up to 300°C. The high temperature practically eliminates the fluid platen option and introduces additional requirements on the data acquisition system, such as minimising the effects of temperature variations on strain measurement. In mac^{2T} the loading platens are made of temperature resistant steel (Durehete 1055, 20CrMoVTiB4-10), whereas the thermal effects on the strain measurements are minimised by using a contactless, laser interferometer system.
- (iv) Complex multi-stage experiments following arbitrary pre-programmed loading paths with simultaneous temperature cycling. This requirement reflects the desire to generate experimental data for calibrating generalised 3D models able to simulate the response of the material to any combination of loading paths and temperature histories. This was achieved by a custom built system for data acquisition and control with dedicated control software specially developed to meet this requirement.

Other important design requirements were: (v) to minimise the friction on the platen-specimen interface, and (vi) to ensure that the three stresses are delivered centrally on the six faces of the specimen.

Loading and Load Measurement

The load in mac^{2T} is delivered by three 4 MN hydraulic actuators installed in independent, diagonally interlaced loading frames (Fig. 2). This design was chosen to minimise the snap-back potential of the loading frames without increasing the demand on the unloading speed of the servo-hydraulic control system. The high stiffness of the frames was achieved by keeping the tensile bars and the crossheads as short as possible, while allowing sufficient room for the specimen to be installed and removed. Each frame comprises two 200 mm

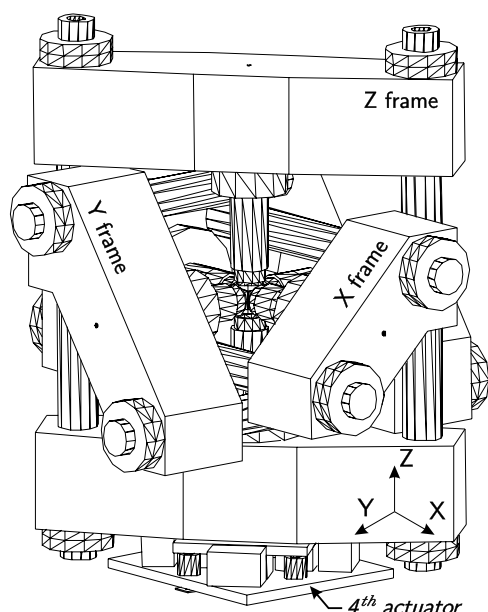


Fig. 2. mac^{2T} loading frames and 4th actuator

diameter steel tensile bars and two 550 mm thick, rolled steel crossheads, one solid, used as a reaction block (supporting the load cell), the other containing the fluid chamber for the hydraulic actuator (Fig. 3). This represents an alternative design solution to that adopted in the six-actuator 250 kN ASTREE apparatus at LMT-Cachan [22].

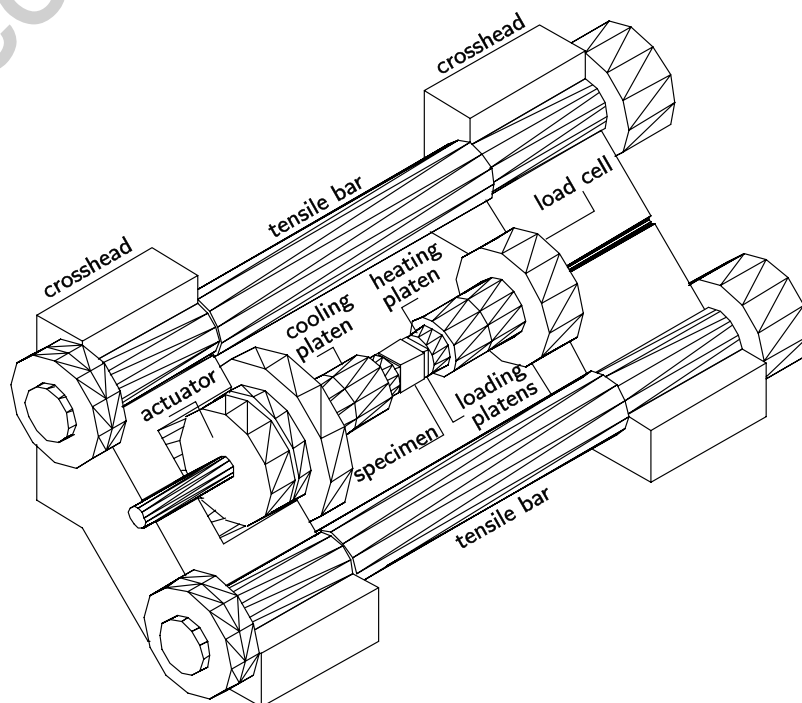
The load to the specimen is delivered by 200 mm diameter rams, through a system of cooling, heating and loading platens. In each test, a set of six new 1 mm

thick steel tiles with 0.25 mm PTFE pads are placed between the loading platens and the concrete specimen to reduce friction-induced shear stresses at the interface. The loading platens have a spherical seat arrangement to accommodate minor departures in the specimen from a right-regular cube. The 95 mm square loading surface is smaller than the surface of the specimen to prevent contact between adjacent loading platens.

One of the actuators (X) has a 180 mm stroke which, when fully retracted, leaves enough space for installing and removing the specimen. The stroke of the other two actuators is 60 mm. The pressure in the system is provided by a 30 MPa hydraulic power unit, which can generate loads up to 3.61 MN (or $\sigma = 400$ MPa over a $95 \times 95 \text{ mm}^2$ area).

A nominally uniform stress field in a (homogenous) specimen can only be achieved by (i) eliminating the friction on the platen-specimen interface, (ii) ensuring that the central axes of the loading platens always cross at the centroid of the specimen and (iii) using precisely machined, right regular cubic specimens. In previous rigid-platen rigs the friction has been reduced by using either greased polyethylene pads (New Mexico [15]) or brush platens (Eindhoven [17]). Polyethylene pads cannot sustain the high temperature levels required in mac^{2T} and, although brush platens have been successfully applied in high-temperature testing (in the biaxial Braunschweig rig [19]), they would not be suitable for post-peak testing where large post-peak deformations may lead to bending and buckling

Fig. 3. Cross-section of loading frame X



of the brushes. PTFE remains stable at temperatures up to 400°C, with very little change in the friction coefficient for temperatures between 20°C and 327°C. The 0.25 mm PTFE pads, eventually selected for mac^{2T} , showed no signs of damage at temperatures up to 300°C and stresses of up to 330 MPa.

It would be inappropriate to attempt a highly detailed FE prediction of the actual stress field operating within a specimen, as the heterogeneity resulting from the stiff aggregate particles (of unknown position) creates local stress gradients that mask any non-uniform effects from the platen-specimen contact. The decision taken here (common to all such multiaxial experimental work with structural concrete) has been to report nominal stress and strain measures when presenting the results.

Eccentric loading is prevented by supporting the two horizontal frames (X and Y) on low friction roller bearings, which allow free movement of the crossheads in the horizontal plane. Movement of the centroid of the specimen in the vertical direction (as a result of elastic deformations of the load cell, platens and loading frame) is prevented by active control of the vertical loading frame (Z) position during the tests. This is achieved by an array of 4 linked servo-hydraulic actuators (collectively known as the 4th actuator, installed beneath the Z frame (see Fig. 2) and controlled by the difference in the displacements measured at the opposite faces of the specimen. This system contrasts with the ASTREE rig at LMT-Cachan [22], where an actuator and a load cell are used to control/monitor the position/load on each side of the specimen. mac^{2T} lifts/lowers the entire Z frame to ensure that the specimen centroid remains at the same position within the laboratory throughout the test. Differences in the axial forces from one side of the specimen to the other are minimised through the use of the low friction membranes at the platen-specimen interfaces.

The crossheads of the X and Y load frames are supported on 4 reinforced concrete seats bolted to a heavily reinforced concrete slab (Fig. 4). The effects of vibrations induced by machinery operating in the laboratory are reduced by supporting the slab on three columns founded at the lower level (basement) and completely isolated from the floor. Two reinforced concrete columns and an upper crossbeam support vertical guides which keep the Z frame in a vertical plane during re-positioning by the 4th actuator.

The applied forces are measured by using three 4 MN rated, high precision (± 4 kN) load cells, installed on the reaction side of each frame. These are low-profile (150 mm), shear-type, 400 mm diameter units,

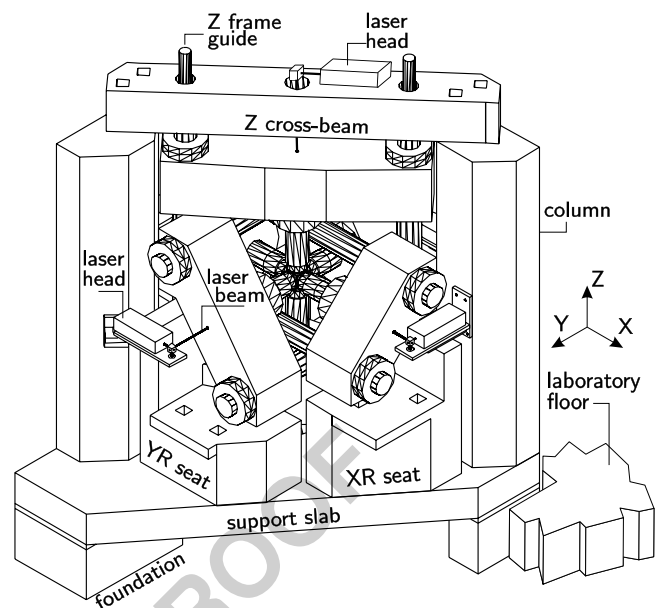


Fig. 4. mac^{2T} load frames and supports

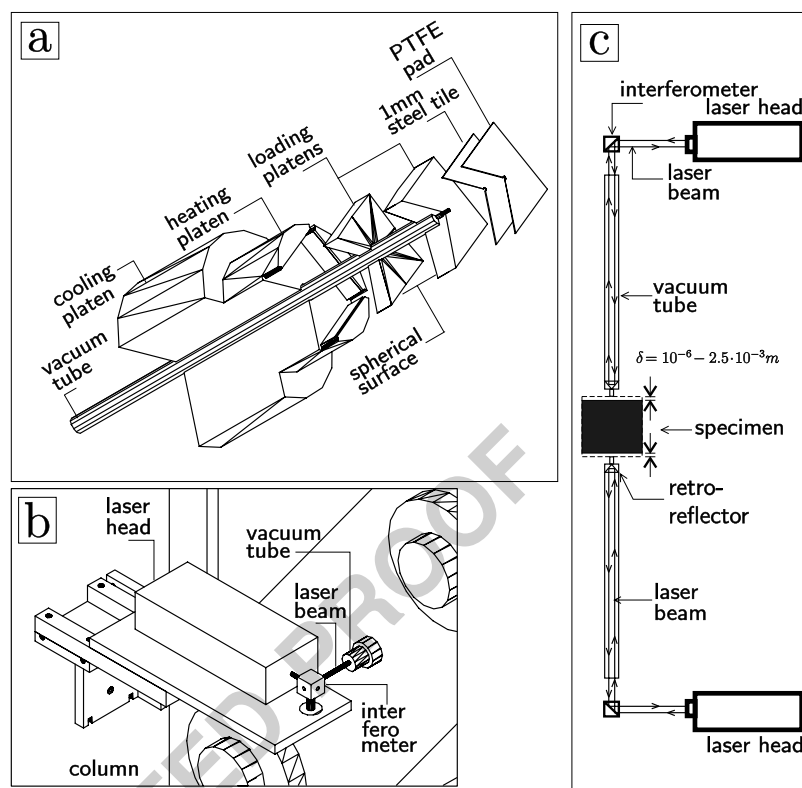
each equipped with two full-bridge strain gauge arrangements. The signal from each bridge is acquired independently and then averaged to provide the process variable for the closed-loop control system (when an axis is under load control). The three load cells are calibrated in the rig, using a separate 3.5 MN load cell, which is itself regularly calibrated at the UK National Physical Laboratory.

Displacement and Strain Measurement

Positioning of the actuators, all the strain measurements and the strain control during the tests are realised by using a system of 6 laser interferometer units. Each unit comprises a laser head (Hewlett Packard, model 5529), a linear interferometer, a linear retro-reflector and a programmable PC calibrator board installed in a dedicated (slave) PC.

The retro-reflectors are installed in 18 mm diameter stainless steel tubes, evacuated to 10^{-5} bar, inserted in the 25 mm diameter holes which run through the actuator rams and platens (Fig. 5), as well as through the load cells and crossheads on the reaction side. The vacuum is necessary to reduce turbulent movement of hot air which disturbs the laser beams and may interrupt the measurements. At the specimen end of each of these tubes there is a 5 mm diameter steel pin, which protrudes through the loading platens (including the 1 mm protective steel tile and 0.25 mm PTFE pad) and contacts the face of the specimen directly. Within the tube, the retro-reflector is secured in position at a distance of 47 mm from the tip of the pin. It is just over

Fig. 5 System for strain measurement and displacement control: **(a)** platens with installed vacuum tubes, **(b)** mounting of lasers and **(c)** schematic diagram of laser interferometer system



this length that thermal expansions and contractions of the pin and the tube have to be calibrated-out during the heating/cooling phases of a test. This setup gives more accurate and reliable results than systems in which the strains are calculated from displacements measured at the ends of long rods [19, 20].

This system is capable of measuring large displacements with 10^{-6} m accuracy, making it suitable for positioning of the actuators (controlling up to 150 mm of pre-contact movement) and the vertical frame (using the 4th actuator) as well as for strain measurements and strain control during the tests (with displacement rates as low as $10^{-5} \text{ m} \cdot \text{min}^{-1}$). In both cases the values obtained from the displacement measurement system are used to calculate the process variables for the servo-control system. Strains in the specimen are calculated from the difference between the displacements measured on the opposite faces of the specimen.

Heating and Cooling

Heat in the rig is generated by a set of six 240 W ceramic band heaters wrapped around the 140 mm diameter steel heating platens [Fig. 5(a)]. Heat is transferred by conduction through the Durehete 1055 (20CrMoVTiB4-10) steel loading platens to the speci-

mens. The load-cell and actuator are kept cool by flushing cold water through a network of holes cross-drilled through the 200 mm diameter steel cooling platens [Fig. 5(a)].

Data Acquisition and Control

The system for data acquisition and control of mac^{2T} is integrated into a PC-based solution built around National Instruments hardware and MCC (mac^{2T} Control Centre), a dedicated LabVIEW program for data acquisition and control developed by the first author. The master PC used in the tests is a dual Athlon 2 GHz platform equipped with one 24 bit digital input/output board (DIO), two 16 bit multifunction boards (MIO) and one 12 bit analogue output module (AO).

All tests in mac^{2T} are monitored by using a total of 49 sensors: (i) 3 load cells (each with 2 independently monitored full-bridge sensor arrangements), (ii) 6 laser interferometer systems for displacement measurement (both position and specimen deformation), (iii) 1 pressure transducer for monitoring the pressure in the 4th actuator, (iv) 6 linear variable displacement transducers (LVDTs) used as a backup displacement measurement system, (v) 6 LVDTs used to monitor the position of the crossheads and

(vi) 24 K-type thermocouples installed on the heating platens (4 per platen).

The signals from all analogue devices (LVDTs, load cell bridges, pressure transducer and thermocouples) are first conditioned, then passed to the analogue IO boards where they are converted into digital data at a rate of $500 \text{ samples} \cdot \text{s}^{-1}$ (multiplexed over 43 channels). In MCC, the acquired data are then averaged in packages of 100 samples at a time. The signals from the laser interferometers are generated as digital data by the six PC calibrator boards installed in the slave PC and transferred to the master PC by the means of digital IO communication controlled from MCC.

The averaged input values and the test control parameters are used for calculating the control variables in the PID (proportional, integral, derivative) modules in MCC. The program outputs are the values of the signals to be sent to the 4 actuator servo-valves and 6 temperature controllers. The analogue (voltage) signals are generated by four 16-bit D/A converters of the MIO boards, for the actuators, and six 12-bit D/A converters of the AO module, for the control of the heaters.

Operation of the Rig

The process of acquiring the data, averaging the values, calculating the control variable and sending the control signal to the servo-valve or temperature controller represents a fully closed control loop. The mac^{2T} rig is operated by 10 independent control loops: 3 for the main actuators, 1 for the 4th actuator and 6 for the temperature controllers. The actual time for closing the loops depends on the ratio between the sampling rate and the number of averages (0.1 s, for the current hardware and software configuration).

In essence, the operation of the rig is controlled by defining three sets of parameters for each of the four actuators: (i) control mode, (ii) process variable (PV), and (iii) rate of change of the PV; and the rate of change of the PV for the temperature controllers.

Control Loops

The three load frame actuators can be operated in either load (LC) or displacement control (DC) mode. The process variable for load control is the load L calculated as an average of the readings from the two bridges of each load cell. The displacement control can be performed by using one of the three different values as process variables: (i) V -the laser measurements of the actuator position, (ii) dV -the laser measurements

of the specimen deformation (difference between the displacements measured at the two opposite faces of the specimen), and (iii) U -the LVDT measurements of the position of the actuators. The diagram of the control loops is shown in Fig. 6.

The V -control is used for positioning the actuators before the beginning of the tests (loading) and after the completion of the tests (unloading). The dV -control is used for displacement control during the tests. The U -control is used in a backup (safety) procedure that is automatically triggered in case any of the laser signals is interrupted. Each load frame is controlled independently, which means that each of the actuators can be under L , V , dV or U -control, regardless of the control mode of the others.

The 4th actuator only operates in displacement control, using one of the three process variables. The six heaters are controlled independently with process variables obtained as average values of the temperature measurements obtained from the 4 thermocouples installed on each of the 6 heating platens.

Modes of Operation and Test Stages

The MCC software is designed to provide two basic modes of operation of the rig: (i) interactive and (ii) automatic. In the interactive mode, the operator controls the rig either by manually setting the control parameters (control modes, PV and rates) for each actuator and temperature controller, or by activating a range of different pre-programmed procedures. In the automatic mode, the program reads an input file at the beginning of the test and performs a series of operations, without the need for further intervention from the operator. The automatic procedure can always be overridden by the operator and switched into interactive mode.

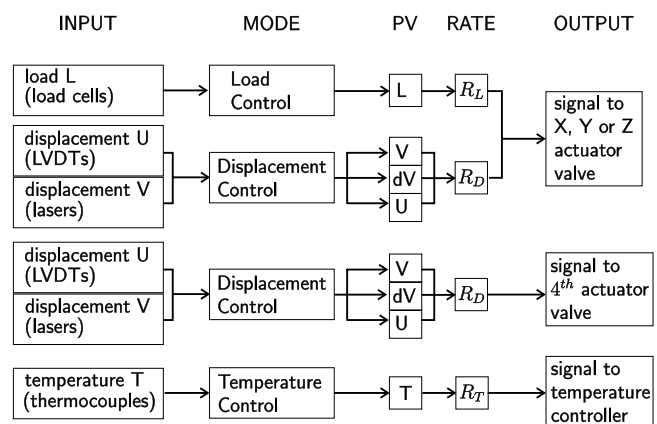


Fig. 6. Operation of mac^{2T} : diagram of control loops

The changes between the control modes are *bump-less* and can be performed at any time during the execution of the test as prescribed by the input file, triggered by the MCC automatically (in case of certain, pre-programmed conditions) or by the operator (in interactive mode). The process variables and rates for each control loop can be also prescribed in the input file, defined by the operator during the test or triggered by the MCC automatically.

Each test is performed in three stages: (i) loading, (ii) testing, and (iii) unloading. Once the specimen is installed in the rig, the operator activates the automatic loading procedure in which the Z frame is lifted into position and the three actuators are extended until the specimen is loaded to contact stress (pre-defined, typically 0.5–1.0 MPa) in all three directions, first Z, then X and finally Y. During this stage, the movement of the Z-frame (4th actuator) and the three loading actuators is controlled by displacements (V-control) with rates decreasing gradually as the platens approach the specimen. Once the contact stress is detected in any of the three directions, the control of that actuator switches to load and the rate of the process variable is set to zero. When all axes are in load control the operator can start the testing stage. Similarly, when the test is finished, the unloading procedure starts by switching the controls to displacement (V) and retracting the actuators in a reverse order: Y, X, Z and finally the 4th actuator, until the Z-frame rests on its base.

In the testing stage the three main actuators are either under load or dV-control, with load/displacement rates prescribed by the pre-programmed test procedure or set by the operator. The 4th actuator is always in dV-control, with variable displacement rates calculated by an MCC module programmed to keep the centroid of the specimen at the same level with the horizontal loading axes during the tests.

Programmed Test Sequences

All mac^{2T} tests can be composed by using six test sequences (procedures) programmed in MCC. Each sequence contains predefined criteria. When these criteria are met, the sequence is completed and the program moves on to the next sequence. The modular structure of the program allows other sequences to be added in the future.

The load cycling in each test is performed by using one of the three different *loading/unloading* procedures: 3LC, 1DC or 2DC.

1. The 3LC procedure, in which the three main actuators are controlled independently in load

control, is used for loading/unloading under specified stress conditions at a safe distance from the peak nominal stress (PNS) surface. The sequence is completed when the load in one axis (*leader*) reaches a pre-defined level.

2. 1DC is a procedure in which one axis (σ_1) is under displacement control with a prescribed displacement rate (R_D), whereas the other two axes are in load control, following σ_1 at preset ratios α_2 and α_3 . The change of σ_1 is monitored at regular time intervals (t_c), and, assuming that the stress rate remains unchanged during two successive intervals ($\Delta\sigma_1^{i+1} = \Delta\sigma_1^i$), the loading rates for the other two directions ($k = 2, 3$) are calculated as: $R_k = [\alpha_k(\sigma_1^i + \Delta\sigma_1^i) - \sigma_k^i]/(t_c A)$, where A is the loading area. This procedure is used for experiments in which one stress (σ_1) is close to the peak, such as triaxial compression ($\sigma_1 > \sigma_2 = \sigma_3$), or tests in which the three stresses are different ($\sigma_1 > \sigma_2 > \sigma_3$).

3. 2DC is similar to the 1DC procedure, but with two *leader* axes in displacement control (with prescribed rates R_{D1} and R_{D2}) and one in load control. The loading rate in the third axis is calculated in the same way as that in the 1DC procedure, but with the stress rate taken as an average of the stress increments measured in the two *leader* axes.

This procedure is used for close-to-peak testing near the extension meridian, where the stresses in two directions are similar while the stress in the third direction decreases or remains constant ($\sigma_1 \approx \sigma_2 > \sigma_3$).

The two DC procedures are used for testing close to peak and in the post-peak region. They are not suitable for lower stress levels where the specimen is still relatively stiff and even low displacement rates in the *leader* axes can produce high loading rates in the load-controlled axes, possibly resulting in serious over/under shooting of the PID controllers and, ultimately, to loss of control. The execution of the DC sequences is controlled by setting limits to the values of (i) the loading stiffness $S = \Delta\sigma_1/\Delta\varepsilon_1$ and (ii) ratio between the current stress and the maximum stress recorded during the sequence $\beta = \sigma_1/\hat{\sigma}_1$; calculated for the *leader* axis (or average of the two *leader* axes in 2DC) at the end of intervals with a pre-defined duration t_c . The limit of the stress ratio β is always set between 0 and 1. If $S_{\text{lim}} > 0$, then the sequence is terminated when $S < S_{\text{lim}}$, before the specimen starts softening (pre-peak tests). If $S_{\text{lim}} < 0$, then the sequence is terminated when the stress σ_1 drops below $\beta_{\text{lim}} \hat{\sigma}_1$ (post-peak tests).

Stress probing procedures are test sequences in which the specimen is loaded/unloaded by a small stress (typically $\Delta \sigma^P = 2 - 3 \text{ MPa}$) in each of the three directions, while the strains in the other two directions are kept constant. The results are used to determine the values of the tangent stiffness and elastic unloading stiffness matrices of the material for a given stress state (at the start of the probing procedure).

4. P3LC is a stress probing procedure in which the three stress probes are performed in load control. When the stress in the probing direction i increases by $\Delta \sigma_i^{Pi}$, the strain in this direction changes to $\varepsilon_i + \Delta \varepsilon_i^{Pi}$. The strains in the other two directions are kept constant ($\Delta \varepsilon_j^{Pi} \approx \Delta \varepsilon_k^{Pi} \approx 0$) while the stresses change by $\Delta \sigma_j^{Pi}$ and $\Delta \sigma_k^{Pi}$, as shown in Fig. 7(a). When the three probes are completed the tangent stiffness matrix \mathbf{D} is calculated from the stress and strain increments measured during the loading parts of the three probes [see Fig. 7(b)]. The elastic unloading matrix \mathbf{D}_u is calculated in a similar way from the values recorded in the unloading branches of the three probes. After completing the three probes, the stresses are returned to their initial levels recorded at the start of the probing sequence, and the program moves on to the next test sequence.
5. P1DC is a probing sequence in which the loading part of the probe in one direction (σ_1) is performed under displacement control with a given rate R_D . This procedure is used in tests where the major principal stress is greater than the other two stresses and close to the PNS ($\sigma_1 > \sigma_2 \geq \sigma_3$). If σ_1 is close to the peak, the loading stiffness of the specimen in the probing direction can be very low (often associated with stress relaxation in the other two directions) and loading to $\sigma_1 + \Delta \sigma_1^{P1}$ can take a long time. If the specimen is softening, then σ_1 will decrease under displacement control. To avoid very slow loading or softening, the time for the loading part of the probe is limited, resulting in $\Delta \sigma_1^{P1} < \Delta \sigma^P$ or even $\Delta \sigma_1^{P1} < 0$ (stress relaxation).
6. P2DC is similar to P1DC, but with two stress probes performed under displacement control. This procedure is used in triaxial extension tests where $\sigma_1 \approx \sigma_2 > \sigma_3$, and the two larger stresses are close to the peak stress levels.

The temperature in the specimen is controlled in all test sequences by specifying the heating rate R_H (in $^\circ\text{C} \cdot \text{min}^{-1}$) and limit temperature T_L . When T_L is reached the program sets R_H to 0.

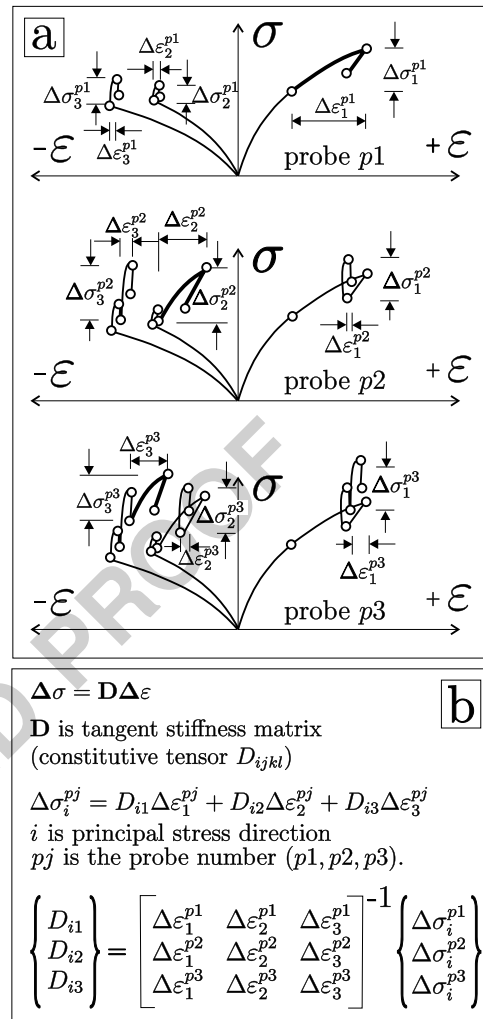


Fig. 7. Stress probing: (a) test sequence and (b) experimental determination of stiffness matrices

Experimental Testing in mac^{2T}

A typical elevated temperature test in mac^{2T} is performed in two phases: (i) *conditioning* and (ii) *deviatoric loading*.

Conditioning Phase

In the *conditioning* phase the specimen is subjected to temperature changes with or without load. When loaded, the specimens are subjected to moderate (service) stresses, typically no higher than 50% of the uniaxial compression strength of the material (f_c). The temperature is either increased monotonically to \hat{T} (up to 300°C) or applied in cycles between ambient and \hat{T} , at constant heating/cooling rates between 0.1 and $3^\circ\text{C} \cdot \text{min}^{-1}$. During the heating and cooling stages the temperature inside the specimen lags behind that measured in the platens. Calibration tests on speci-

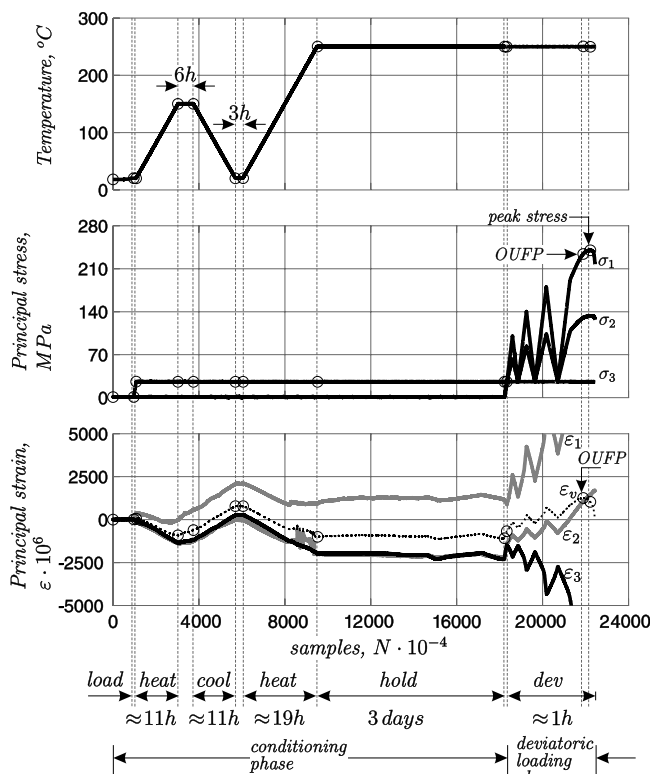


Fig. 8. Typical elevated temperature test in mac^{2T}: histories of temperature, stress and strain

mens with embedded thermocouples showed that the temperatures within the specimen depended on the heating rate and the moisture content of the concrete. For 2 year old concrete kept at room conditions, heated to $\hat{T} = 250^\circ\text{C}$ at $2^\circ\text{C} \cdot \text{min}^{-1}$, the temperatures within the specimen were 190°C , 10 mm from the surface, and 180°C , at the centroid, when the platens first reached 250°C . After maintaining the platen temperature at 250°C for 2 hours, the specimen centre reached 236°C . All *conditioning* phases in the elevated temperature tests performed in mac^{2T} included a period of at least 24 hours holding at constant temperature of 250°C , at which time the specimen attained a steady state $\approx 248^\circ\text{C}$.

Load-then-heat (L-H) tests are used for investigating the load induced thermal strains (LITS), a phenomenon of particular importance for fire engineering and design of concrete structures in nuclear power plants. After each heating and cooling cycle the specimen is held under steady state conditions for short periods until it reaches thermal and hygral equilibrium. In some tests the heating to \hat{T} is followed by longer periods of steady state (up to 5 days), in order to measure creep at constant (elevated) temperature. Heat-then-load (H-L) tests are used to determine drying shrinkage (needed for separating LITS from

total strains) and to provide a reference for assessing the effects of heat-load regimes on the material behaviour under multiaxial stress.

The time histories of temperature, stress and strain from a typical mac^{2T} L-H test are shown in Fig. 8. The specimen is first loaded in uniaxial compression to 26 MPa, then heated to 150°C , cooled to 20°C , heated to 250°C , and held under steady-state conditions for 3 days before starting the *deviatoric loading* phase.

Deviatoric Loading Phase

The influence of different loading and heating-cooling regimes in the *conditioning* phase on the properties of the material under multiaxial loading are investigated in the second, *deviatoric loading*, phase of the tests.

In the simplest tests, the specimen is loaded in one deviatoric plane (between Lode angles $\pi/6$ and $-\pi/6$), in several cycles with gradually increasing stress

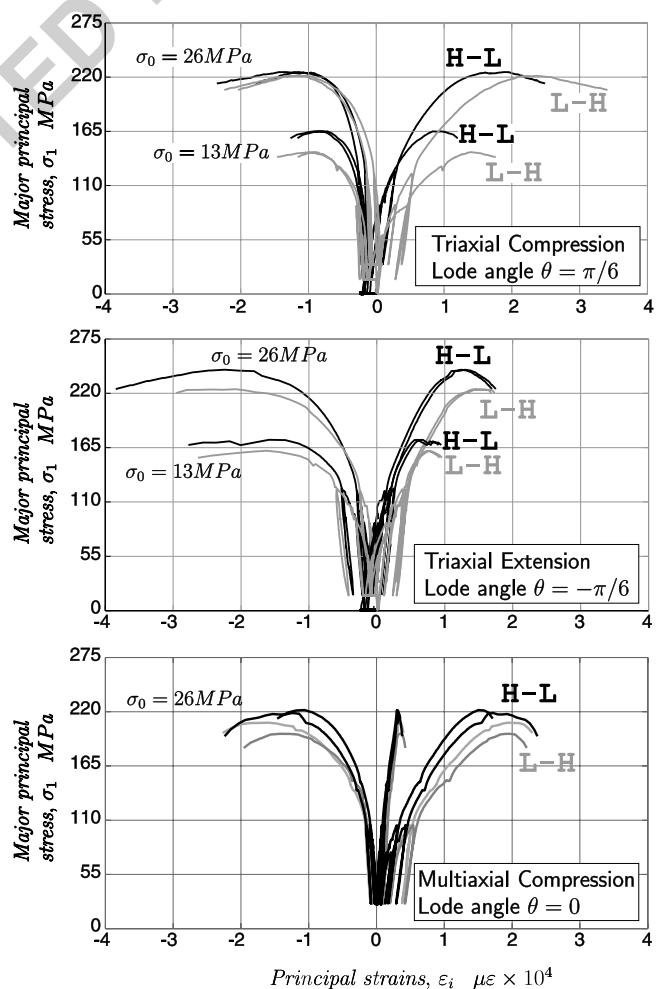


Fig. 9. Simple deviatoric loading test in mac^{2T}: stress-strain graphs recorded after heat-load (H-L) and load-heat (L-H) conditioning at two different levels of hydrostatic confinement σ_0

magnitudes, followed by monotonic loading to peak stress (Fig. 9). These tests provide data on the relationship between heating, cooling and loading (\dot{T} , heating-cooling rates, heat-load sequence, and stress state during heating-cooling) and multiaxial strength of the material [23], tangent stiffness, elastic unloading stiffness, pre-peak volumetric expansion (or OUF—onset of unstable fracture propagation), plastic flow and softening behaviour of the material.

More complex deviatoric loading tests include (i) deviatoric load cycles at fixed Lode angles but varying hydrostatic confinement levels and (ii) stress probes at different stress levels in each deviatoric cycle.

In Fig. 10 are shown the loading path and stress-strain response recorded in a triaxial compression test ($\theta = \pi/6$, $\sigma_1 > \sigma_2 = \sigma_3$). The load was applied in six deviatoric planes (normal to the hydrostatic axis ξ), at increasing levels of hydrostatic confinement. The test in each cycle i was carried out in 4 steps: (1) load hydrostatically to a predefined level σ_0^i , (2) load in a deviatoric plane to $\sigma_1 = 0.975\hat{\sigma}^i$, (3) perform probes at

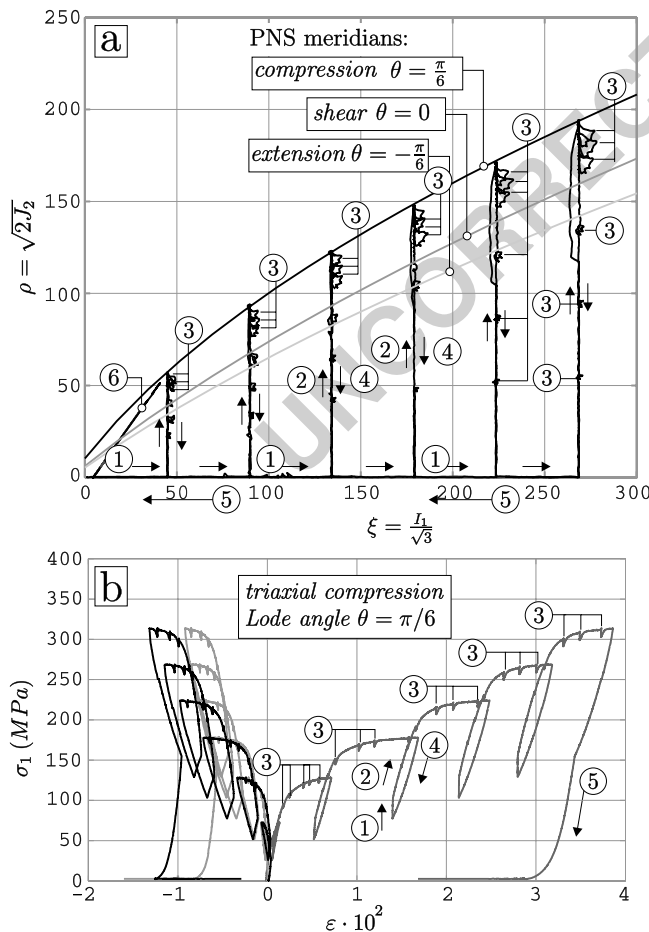


Fig. 10. Complex deviatoric loading in mac^{2T}: (a) loading path and (b) stress-strain response of the specimen under multiaxial compression. $I_1 = \text{tr}[\sigma]$ and $2J_2 = \text{tr}[s^2]$

$$Q_{jk} = n_i D_{ijkl} n_l$$

Q_{jk} is acoustic tensor

D_{ijkl} is constitutive tensor

n_i is direction vector

$$n_1 = \begin{pmatrix} 1 \\ 0 \\ 0 \end{pmatrix} \quad n_2 = \begin{pmatrix} 0 \\ 1 \\ 0 \end{pmatrix} \quad n_3 = \begin{pmatrix} 0 \\ 0 \\ 1 \end{pmatrix}$$

Fig. 11. Acoustic tensor surface calculated from experimentally determined stiffness matrices

6 stress levels $\sigma_1 = 0.6, 0.7, 0.8, 0.9, 0.925$ and $0.95\hat{\sigma}^i$, and (4) unload to σ_0^i . After completing the six loading cycles, the specimen was unloaded along the hydrostatic axis (step 5) and tested under σ_3 compression ($\sigma_1 = \sigma_2 = 3\text{MPa}$) to determine the residual strength of the material (step 6).

Performing a series of small compression *probes* in each of the three orthogonal directions, while maintaining strains fixed in the other directions, allows the isotropic upper 3×3 sub-matrix of the 6×6 constitutive $[D]$ matrix to be estimated [Fig. 7(b)]. The remaining terms of the $[D]$ matrix were calculated by adopting the original elastic shear modulus. This could have been estimated, for an equivalent isotropic material, from the altered mean Young's modulus and mean Poisson's ratio. However, the effect of not changing the shear modulus was shown to be near-negligible when examining an equivalent elasto-plasticity model. By calculating the acoustic tensor from this matrix, a measure of impending material instability can be determined [24]. This measure (the determinant of the acoustic tensor) has both direction and magnitude, thus it may be represented graphically (Fig. 11) by a surface which starts out as being spherical and evolves (collapses) into a form where the radius becomes zero in the direction normal to the orientation of a newly formed discontinuity surface. Such results give a detailed picture of the material behaviour under multiaxial compression needed for construction of advanced constitutive models.

Conclusions

The new mac^{2T} facility was developed to overcome the lack of high quality experimental data on the behav-

behaviour of concrete under true triaxial compression, under relatively high levels of confinement, at both ambient and elevated temperature. The fully automated programmable control system allows multi-stage experiments to be carried out by following complex load paths and temperature histories, at any Lode angle and in the post-peak range. These tests provide new macroscopic data needed to construct advanced constitutive models for simulating the response of concrete under generalised stress states. The observed effects of different heating and loading regimes on the evolving mechanical properties provide insight into the stress and temperature-induced changes in the material fabric at a lower, microscopic, level.

Acknowledgments The authors are most grateful to the consortium of companies from the British nuclear industry and the Higher Education Funding Council for England (HEFCE) for supporting the construction and operation of the mac^{2T} facility.

References

- Kupfer HB, Hilsdorf HK, Rusch H (1969) Behaviour of concrete under biaxial stresses. *J ACI* 66(8):656–666.
- Liu TC, Nilson AH, Slate FO (1972) Stress-strain response and fracture of concrete in uniaxial and biaxial compression. *J ACI* 69(5):291–295.
- Gerstle KH, Aschl H, Bellotti R, Bertacchi P, Kotsovos MD, Ko H-Y, Linse D, Newman JB, Rossi P, Schickert G, Taylor MA, Traina LA, Winkler H, Zimmerman RM (1980) Behaviour of concrete under multiaxial stress states. *J Eng Mech, ASCE* 106:1383–1403.
- Franklin JA, Hoek E (1970) Developments in triaxial testing equipment. *Rock Mech* 2:223–228.
- Chern JC, Yang HJ, Chen HW (1992) Behaviour of steel fiber reinforced concrete in multiaxial loading. *ACI Mater J* 89(1):32–40.
- Attard MM, Setunge S (1996) Stress-strain relationship of confined and unconfined concrete. *ACI Mater J* 93(5):432–442.
- Imran I, Pantazopoulou SJ (1996) Experimental study of plain concrete under triaxial stress. *ACI Mater J* 93(6):589–601.
- Newman JB (1973) Deformation behaviour, failure mechanisms and design criteria for concrete under combinations of stress, Part IV, PhD Thesis, University of London, 1–583.
- Jamet P, Millard A, Nahas G (1984) Triaxial behaviour of a micro-concrete complete stress-strain curves for confining pressures ranging from 0 to 100 MPa. In: RILEM-CEB International Conference Concrete under Multiaxial Conditions, INSA Toulouse, 1984, Vol. 1, 133–140.
- Smith SS, Willam KJ, Gerstle KH, Sture S (1989) Concrete over the top, or: is there life after Peak? *ACI Mater J* 86(5):491–497.
- Li Q, Ansari F (1999) Mechanics of damage and constitutive relationships for high-strength concrete in triaxial compression. *J Eng Mech ASCE* 125(1):1–10.
- Sfer D, Carol I, Gettu R, Etse G (2002) Study of the behaviour of concrete under triaxial compression. *J Mech Eng ASCE* 128(2):156–163.
- Bellotti R, Rossetti P (1991) Cylinder tests: experimental technique and results. *Mat Struct* 24:45–52.
- Vu XH, Gabet T, Malecot Y, Daudeville L (2005) Experimental analysis of concrete behaviour under severe triaxial loading. *Proc. McMat2005, Joint ASME/ASCE/SES Conference on Mechanics and Materials*, Baton Rouge, Louisiana, paper 247, 1–6.
- Mills LL, Zimmerman RM (1970) Compressive strength of plain concrete under multiaxial loading conditions. *ACI Journal*, October 1970, 802–807.
- Scavuzzo R (1982) Behaviour of concrete under multiaxial load histories. MSc Thesis, University of Colorado.
- Van Mier JGM (1984) Strain softening of concrete under multiaxial loading conditions. PhD Thesis, University of Eindhoven.
- Van Mier JGM, Vonk RA (1991) Fracture of concrete under multiaxial stress-recent developments. *Mat Struct* 24:61–65.
- Ehm C, Schneider U (1985) The high temperature behaviour of concrete under biaxial conditions. *Cem Concr Res* 15:27–34.
- Thienel K-Ch, Rostásy FS (1996) Transient creep of concrete under biaxial stress and high temperature. *Cem Concr Res* 26(9):1409–1422.
- Bazant ZP, Prasannan S (1986) High-temperature triaxial torsional creep tests of concrete at various hygral conditions. *Nucl Eng Des* 94:137–151.
- Calloch S, Marquis D (1999) Triaxial tension-compression tests for multiaxial cyclic plasticity. *Int J Plast* 15:521–549.
- Petkovski M, Crouch R, Waldron P (2005) Multiaxial creep and damage under elevated temperature. *Concreep 7—International conference on creep, shrinkage and durability of concrete and concrete structures*, Nantes, 12–14 September 2005, paper CC7-121, in press.
- Rudnicki JW, Rice JR (1975) Conditions for localization of deformations in pressure sensitive dilatant materials. *J Mech Phys Solids* 23:371–394.